The P2X$_7$ Receptor Channel Pore Dilates under Physiological Ion Conditions

Zonghe Yan, Shuo Li, Zhaodong Liang, Melanija Tomić, and Stanko S. Stojilkovic

Section on Cellular Signaling, Program in Developmental Neuroscience, National Institute of Child Health and Human Development, National Institutes of Health, Bethesda, MD 20892

Activation of the purinergic P2X$_7$ receptor leads to the rapid opening of an integral ion channel that is permeable to small cations. This is followed by a gradual increase in permeability to fluorescent dyes by integrating the actions of the pannexin-1 channel. Here, we show that during the prolonged agonist application a rapid current that peaked within 200 ms was accompanied with a slower current that required tens of seconds to reach its peak. The secondary rise in current was observed under different ionic conditions and temporally coincided with the development of conductivity to larger organic cations. The biphasic response was also observed in cells with blocked pannexin channels and in cells not expressing these channels endogenously. The biphasic current was preserved in N-terminal T15A, T15S, and T15V mutants that have low or no permeability to organic cations, reflecting enhanced permeability to inorganic cations. In contrast, the T15E, T15K, and T15W mutants, and the Δ18 mutant with deleted P2X$_7$ receptor–specific 18–amino acid C-terminal segment, were instantaneously permeable to organic cations and generated high amplitude monophasic currents. These results indicate that the P2X$_7$ receptor channel dilates under physiological ion conditions, leading to generation of biphasic current, and that this process is controlled by residues near the intracellular side of the channel pore.

INTRODUCTION

The purinergic P2X receptors (P2XRs) are a family of ligand-gated ion channels composed of seven subunits, termed P2X$_{1-7}$ (Egan et al., 2004), and these subunits assemble as homo- or heterotrimers to make functional receptors (Nicke et al., 1998, 2005). The P2X$_7$R subunit, initially cloned from a rat brain cDNA library, shares an overall membrane topology with the other members of this family of receptors; it contains two putative pore-forming transmembrane segments, a large cysteine-rich ligand-binding extracellular domain, and intracellularly located N and C termini (Surprenant et al., 1996). Structurally, the receptor is distinguished from other members of P2XRs by its long intracellular C-terminal tail containing multiple protein and lipid interaction motifs, and a cysteine-rich 18–amino acid segment. The P2X$_7$R also requires at least a 100-fold higher ATP concentration for activation than is required for other P2XRs, and removal of divalent cations increases agonist potency (Ferrari et al., 2006). Extracellular cations and chloride have complex effects on the channel gating (Virginio et al., 1997; Gudipaty et al., 2001; Li et al., 2003, 2005; Riedel et al., 2007b). Furthermore, during sustained activation, P2X$_7$R can elicit a wide range of intracellular signaling responses that are usually associated with the G protein–coupled receptors (Dubyak, 2007).

Finally, P2X$_7$R operates as a nonselective cationic channel during initial agonist application, but with prolonged application, the receptor also provides a permeation pathway to molecules with a molecular weight of up to ∼800 D, including the fluorescent dye YO-PRO-1, a process termed cell "permeabilization."

Initially, it was suggested that the bi-functional permeation properties of P2X$_7$R reflect a dilation of the integral pore of the channel. Thus, the cation-permeable recombinant channel is activated rapidly (within milliseconds) after application of agonists, followed by a gradual (within seconds to minutes) increase in permeability to NMDG$^+$ and fluorescent dyes, both occurring at comparable rates (Surprenant et al., 1996; Chessell et al., 1997; Michel et al., 1999; Gudipaty et al., 2001). It was further suggested that a progressive dilation of the ion-conducting pathway during prolonged agonist application is not a unique feature of the P2X$_7$R, but also occurs in cells expressing P2X$_2$R and P2X$_4$R (Khakh et al., 1999; Virginio et al., 1999). However, the development of NMDG$^+$ permeability and the uptake of fluorescent dyes were not always detected in cells responding to application of agonist with inward currents (Petrou et al., 1997; Klapperstuck et al., 2000). Furthermore, the permeability to NMDG$^+$ was reduced in low Na$^+$-containing medium and was completely abolished in cells bathed in normal extracellular Na$^+$, questioning the pore dilation hypothesis (Jiang et al., 2005). In addition, the uptake of fluorescent dyes was not affected in cells expressing P2X$_7$R in which the receptor-specific

The Rockefeller University Press $30.00
J. Gen. Physiol. Vol. 132 No. 5   563–573
www.jgp.org/cgi/doi/10.1085/jgp.200810059

563

C-terminal 18–amino acid sequence was deleted, but mutant was not permeable to NMDG[+], suggesting that YO-PRO-1 entry occurs through a separate pathway than NMDG[+] (Jiang et al., 2005). Furthermore, cells expressing mutant P2X$_7$R that was truncated at residue 581 had negligible ethidium uptake and normal current responses (Smart et al., 2003). Finally, the coupling of P2X$_7$R to pannexin-1 channels was suggested to account for cellular entry of fluorescent dyes (Pelegrin and Surprenant, 2006).

Here, we addressed the hypothesis that P2X$_7$R pore dilates independently of the expression of pannexin-1 channels. The rat P2X$_7$R was expressed in human embryonic kidney (HEK) 293 cells and gonadotropin-releasing hormone-secreting (GT1) cells, which express pannexin-1 channels endogenously, as well as in C6 glioma cells, which do not express pannexins. In all cell types, P2X$_7$Rs responded to initial agonist application with a rapid growth of inward current that peaked within milliseconds. This response was accompanied by an additional rise that required tens of seconds to be completed. Our results also suggest that a transition from a closed to an opened state of the channel pore accounts for the rapid rise in current, whereas a transition from an opened to a dilated state accounts for the secondary growth of current. The pore dilation occurs in cells bathed in physiological solution, requires higher agonist concentrations, and is controlled by residues near the intracellular side of the channel pore.

MATERIALS AND METHODS

Site-directed Mutagenesis, Cell Culture, and Transfection

The pIRES2-EGFP P2X$_7$ construct (He et al., 2003) was used as a template for production of plasmids containing specific amino acid residue point mutations of P2X$_7$ cDNA using the Quik-Change II XL site-directed mutagenesis kit (Stratagene). The mutagenic oligonucleotide primers were synthesized and PAGE purified by Integrated DNA Technology. Production of the correct mutations and absence of coding errors in these constructs were verified by dye terminator–cycle sequencing (PerkinElmer; performed by Veritas, Inc.). Large-scale plasmid DNAs were prepared using a QIAfilter Plasmid Maxi kit (QIAGEN). HEK293, C6, and GT1 cells were used for the expression of wild-type (WT) and mutant P2X$_7$ receptors, as described previously (He et al., 2003; Yan et al., 2006). HEK293 and C6 cells (American Type Culture Collection) were routinely maintained in Dulbecco's modified Eagle's medium containing 10% (vol/vol) fetal bovine serum (Invitrogen) and 1% (vol/vol) penicillin-streptomycin liquid (Invitrogen) in a tissue culture incubator. GT1 cells (provided by R.I. Weiner, University of California, San Francisco, San Francisco, CA) were cultured in Dulbecco's modified Eagle's medium/Ham's F-12 medium (1:1) containing 10% (vol/vol) fetal bovine serum and 100 µg/ml gentamicin (Invitrogen). For electrophysiological measurements, cells were grown on 35-mm dishes at a density of 0.5×10^6 cells per dish, whereas for imaging studies GT1 cells were grown on 25-mm coverslips placed in 35-mm dishes at a density of 0.1×10^6 cells per dish. Transfection was conducted 24 h after plating the cells using 2 µg DNA and 5 µl

Lipofectamine 2000 reagent (Invitrogen) in 2 ml of serum-free Opti-MEM. After 4.5 h of incubation, the transfection mixture was replaced with normal culture medium, and cells were cultured for an additional 24–48 h. For electrophysiological measurements, transfected cells were mechanically dispersed and re-cultured on 35-mm dishes for 2–10 h.

Current Measurements

Whole cell patch clamp recordings were performed using single cells at room temperature using an Axopatch 200B amplifier (MDS Analytical Technologies), as previously described (Yan et al., 2005). Patch electrodes, fabricated from borosilicate glass (type 1B150F-3; World Precision Instruments, Inc.) using a Flaming Brown horizontal puller (P-97; Sutter Instrument Co.), were heat polished to a final tip resistance of 3.5–5.5 MOhm. All current records were programmed, captured, and stored using the pClamp 8.0 software packages in conjunction with the Digidata 1322A A/D converter (MDS Analytical Technologies). Experiments were performed on single cells with an average capacitance of 10 pF. Unless otherwise stated, membrane potential was held at −60 mV. Current voltage relations were used to estimate changes in reversal potential during agonist application and were obtained by voltage ramps from −80 to +80 mV twice per second during 50 s. Patch electrodes were filled with solution containing 145 mM NaCl, 10 mM EGTA, and 10 mM HEPES; the pH was adjusted with 10 M NaOH to 7.35. The osmolarity of this solution was 305 mOsM. The regular Krebs-Ringer (KR)-like bath buffer contained 147 mM NaCl, 3 mM KCl, 1 mM MgCl$_2$, 2 mM CaCl$_2$, 10 mM glucose, and 10 mM HEPES; the pH was adjusted to 7.35 with 10 M NaOH. For some experiments, 90 or 100% Na$^+$ was replaced with mM NMDG$^+$ or 2-(methylamino)ethanol (NMEA$^+$), and the solution pH was adjusted to 7.35 with HCl (Na$^+$/NMDG$^+$-KR buffer and NMDG$^+$-KR buffer, respectively). We also used a buffer containing only 155 mM NMDG, 10 mM glucose, and 10 mM HEPES (NMDG$^+$ buffer). The osmolarity of these solutions were 295–305 mOsM. ATP and Bz-ATP solution was daily prepared in bath buffer with pH properly readjusted, applied using either an Ultrafast Solution-Switching System (LSS-3200; EXFO Burleigh Products Group Inc.) that was simultaneously program controlled by pClamp 8.0 software through a PZ-150M Amplifier (Yan et al., 2006) or a RSC-200 Rapid Solution Changer (Biological). Cells with EGFP fluorescence were identified before immersing the electrode in bath solution for gigaohm seal.

Fluorescence Imaging

Transfected GT1 cells plated on 25-mm coverslips were bathed in KR medium containing 2.5 µM of either Fura-2 AM or Fura-FF AM (Invitrogen) for 1 h at room temperature. After washing the coverslips with the dye-free KR media, they were mounted on the stage of an Axiovert 135 microscope (Carl Zeiss, Inc.) attached to an Attofluor Digital Fluorescence Microscopy System (Atto Instruments). Cells were examined under a 40× oil immersion objective during exposure to alternating 340- and 380-nm excitation beams, and the intensity of light emission at 520 nm (F_{340} and F_{380}) was followed in several single cells simultaneously at the rate of one point per second. For YO-PRO-1 uptake, cells were loaded with Fura-2 and subsequently exposed to 5 µM YO-PRO-1 (Invitrogen) in KR medium. The same concentration of YO-PRO-1 was present throughout the experiment, and the experimental setup was identical except for the dichroic mirror and the excitation filters. Fluorescence was observed upon excitation with alternating 380- (Fura-2) and 488-nm (YO-PRO-1) beams. Only cells with low basal F_{488} and cells that showed decreased F_{380} in response to agonist, corresponding to an increase in intracellular calcium concentrations ($[Ca^{2+}]_i$), were further analyzed for changes in F_{488}, corresponding to YO-PRO-1

uptake. YO-PRO-1 fluorescence intensity is expressed in arbitrary units (0–255).

Calculations

Whenever appropriate, the data were presented as mean ± SEM values. Significant differences, with $P < 0.01$, were determined by Mann-Whitney test using GraphPad InStat 3.05.

RESULTS

Patterns of Agonist-induced Currents

Three cell types, HEK293, GT1, and C6 cells, were used in our experiments. When these cells were bathed in KR buffer containing 147 mM NaCl, 3 mM KCl, 2 mM $CaCl_2$, 1 mM $MgCl_2$, 10 mM HEPES, and 10 mM glucose, neither ATP nor BzATP generated current, indicating that in our experimental conditions these cells do not express native P2XRs. In contrast, all cell types transfected with the WT $P2X_7R$ construct responded to BzATP with generation of current. The peak amplitude of currents in response to 100 µM BzATP application was comparable in HEK293 and GT1 cells and significantly smaller in C6 cells. The expression efficiency was also lower in C6 cells. In all cell types, the pattern of current response was dependent on agonist concentration, duration of its application, and number of applications. Unless otherwise specified, electrophysiological recordings were done in HEK293 cells, whereas imaging studies

were performed in GT1 cells because they do not express calcium-mobilizing P2Y receptors.

Cells clamped at -60 mV and stimulated with 100 µM BzATP repeatedly for 0.5–2 s responded with comparable current peaks (Fig. 1 A, left). However, this was not the case when cells were repeatedly stimulated with 100 µM BzATP for 4 s, separated by 2-min intervals. Under such experimental conditions, there was a progressive increase in the peak amplitude of current (Fig. 1 A, right). Growth of current was also evident during longer agonist applications. Fig. 1 B illustrates the pattern of current in response to 4- and 40-s application of 100 µM BzATP. During both applications, there was a rapid rise in current of comparable amplitudes, with the 10–90% rise time completed within 198 ± 9 ms; however, longer exposure to agonist was followed by a secondary growth of current. We termed such a pattern of response as biphasic, and the dotted line in Fig. 1 separates the rapid phase of current growth (I) from the slow phase of current growth (II). To avoid the possible side effects of repetitive exposure to agonists for a prolonged period on pattern of current responses, further recordings were performed only during the initial agonist application (naive receptors).

The averaged ratio between the rapid and slow currents, the latter measured at the end of 40-s applications of 100 µM BzATP, was 1:2.4 (1,011 ± 78 pA vs. 2,390 ± 133 pA; $n = 52$). The biphasic response was also observed
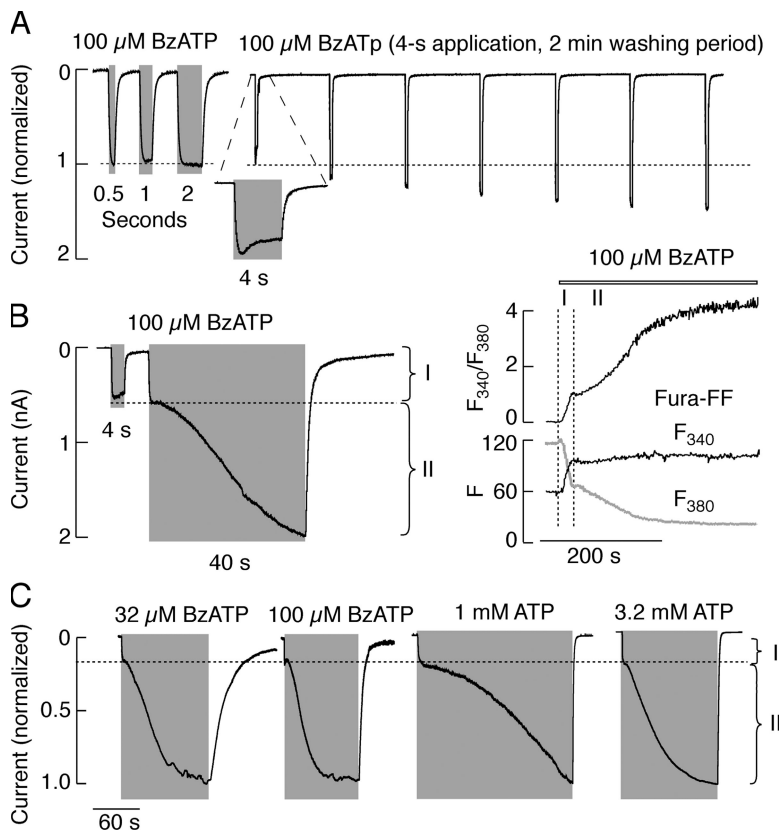
Figure 1. Two phases of activation in rat $P2X_7R$-expressing cells bathed in KR-like buffer. (A) Repetitive short-term stimulation with 100 µM BzATP. Traces shown on the left and right panels are from two different cells. Inset shows the expanded time scale of the initial current response. Horizontal dotted lines indicate the peak amplitude of currents reached during initial agonist application. (B, left) Short-term and subsequent long-term stimulation with 100 µM BzATP. (Right) Calcium response to prolonged application of BzATP in cells loaded with Fura-FF. (C) Dose-dependent effects of BzATP and ATP on the rate of sustained current growth. Traces shown are from different cells during initial agonist application. In B and C, dotted lines separate rapid phase (I) from slow phase (II) in receptor response. Electrophysiological experiments were performed in HEK293 cells, and $[Ca^{2+}]_i$ measurements were performed in GT1 cells expressing recombinant $P2X_7Rs$. Gray areas and bottom numbers indicate duration of BzATP application. Unless otherwise specified, in this and all figures, recordings were performed in cells held at -60 mV. Traces shown are representative of at least five recordings.

in amphotericin-perforated cells, suggesting that the second phase in current growth does not reflect dialysis of cells during the whole cell current recording (not depicted). To rule out other possible artifacts, we used intact cells and single cell calcium measurements. Previous experiments with Fura-2 revealed inability to report high $[Ca^{2+}]_i$ in cells with activated $P2X_7Rs$ (Koshimizu et al., 2000), prompting us to use the less sensitive Fura-FF dye. Because HEK293 cells endogenously express Ca^{2+}-mobilizing P2Y receptors (He et al., 2003), GT1 cells were used as an expression system. In these cells, 100 µM BzATP also induced biphasic $[Ca^{2+}]_i$ response (Fig. 1 B, right), with the averaged ratio between the rapid and slow phase of 1:2.8 comparable to that observed in current measurements (F_{340}/F_{380}: 0.83 ± 0.04 vs. 2.32 ± 0.14; n = 23; basal $[Ca^{2+}]_i$ subtracted). However, the leak of Fura-FF (see Fig. 3) could influence estimates of the F_{340}/F_{380} ratio during sustained agonist application.

When 3–10 µM BzATP was applied for 2 min, only low amplitude monophasic currents were observed, with the amplitude of current determined by agonist concentration (3.2 µM = 19 ± 7.2 pA [n = 4]; 10 µM = 34 ± 5.4 pA [n = 6]). In contrast, cells always responded with the biphasic current when stimulated with 32 and 100 µM BzATP (Fig. 1 C). The secondary growth of current was completed within 80–120 s in cells exposed to 32 µM BzATP, and within 30–70 s in cells exposed to 100 µM BzATP, suggesting that the rate of current growth was determined by agonist concentration. Similar patterns of responses were observed when cells were stimulated with ATP, but with a rightward shift in potency. In low micromolar concentrations, ATP always induced low-amplitude monophasic responses during a 2-min exposure to agonist, with the peak amplitude of current determined by agonist concentration (100 µM = 9.3 ± 2.1 pA [n = 4]; 320 µM ATP = 35.1 ± 3.4 pA [n = 7]). In high millimolar concentrations, ATP induced biphasic responses in all cells, and the rates of secondary current growth were dependent on agonist concentration (Fig. 1 C). In cells stimulated with 3.2 mM ATP, the ratio between the first and second peak values was 1:3.6 (716 ± 132 pA vs. 2622 ± 319 pA; n = 6), comparable to that observed in response to 100 µM BzATP application (see above).

Biphasic Current and Permeability to NMDG+

When 90% of Na^+ was replaced with $NMDG^+$ ($Na^+/NMDG^+$-KR buffer), 100 µM BzATP still induced biphasic current in naive cells held at −60 mV, with kinetics that resembled growth of current observed in cells bathed in Na^+-containing KR medium (Fig. 2 A, left vs. Fig. 1). Under repetitive 485-ms voltage ramp pulses from −80 to +80 mV, delivered twice per second, there was also a progressive increase in the peak amplitude of inward current at −80 mV (Fig. 2 A, middle). Current

voltage curves constructed from ramp voltage commands revealed a shift in reversal potential during the 40-s agonist application from −28.2 ± 0.5 mV to a steady-state of −17.3 ± 1.3 mV (Fig. 2 A, right panel, from left to right). Such a shift was observed in all cells studied (n = 9). We next repeated these experiments in cells bathed in KR medium with $NMDG^+$ replacing all the extracellular Na^+ ($NMDG^+$-KR buffer). Under these ionic conditions, the rate of the secondary growth in current was comparable to that observed in cells perfused with $Na^+/NMDG^+$-KR solution, and the 100 µM BzATP–evoked current reversal potential changed from −36.5 ± 0.3 mV to −24.6 ± 0.8 mV (Fig. 2 B). However, in cells clamped at −60 mV and exposed to BzATP for 40 s, the peak amplitude of current differed in two ionic conditions: (1) $Na^+/NMDG^+$-KR = 1.3 ± 0.2 nA (n = 6), 54% of that observed in cells bathed in KR buffer; (2) $NMDG^+$-KR = 0.59 ± 0.08 nA (n = 4), 24% of that observed in cells bathed in KR buffer. These results suggest that $NMDG^+$ only partially substitutes for Na^+ as the conducted ion.

The time course of 100 µM BzATP–induced current at −60 mV was substantially different in cells perfused with medium containing 155 mM $NMDG^+$, 10 mM HEPES, and 10 mM glucose ($NMDG^+$ buffer) and similar to that reported by others (Jiang et al., 2005). Because the holding potential of −60 mV was more positive than the reversal potential in $NMDG^+$ (−67 ± 0.2 mV), an initial outward current developed rapidly after agonist application, reflecting an outward movement of intracellular Na^+ through the channel pore. The peak amplitude of this current was 309 ± 53 pA (n = 8). This was followed by a decline in current and a shift from outward to inward current within 7 s. A steady-state current was reached within 20 s (Fig. 2 C, left), with the mean value of −241 ± 60 pA (n = 8), 10% of that observed in cells bathed in KR buffer, confirming lower permeability of channel to $NMDG^+$ than to small cations. Furthermore, the reversal potential progressively shifted by +22.5 mV (n = 15; Fig. 2 C, right), compared with the +10.9- and +11.7-mV shifts observed in cells bathed in $Na^+/NMDG^+$-KR and $NMDG^+$-KR solutions, respectively. Finally, the washout of BzATP was not accompanied by receptor deactivation (Fig. 2 C, left), but closed when Na^+ was reintroduced in medium, which is consistent with observations by others (Jiang et al., 2005). In contrast, deactivation of the channel occurs in cells bathed in Na^+-deficient/divalent cation-containing medium (Fig. 2 B), indicating that this process is not specifically dependent on extracellular Na^+, but does require the presence of small cations.

We also examined the permeability of channels to $NMDG^+$ during the rapid and sustained phase of current growth. To do this, cells bathed in KR buffer were stimulated with 100 µM BzATP for 4 and 40 s, followed by replacement of bath medium with $NMDG^+$ medium
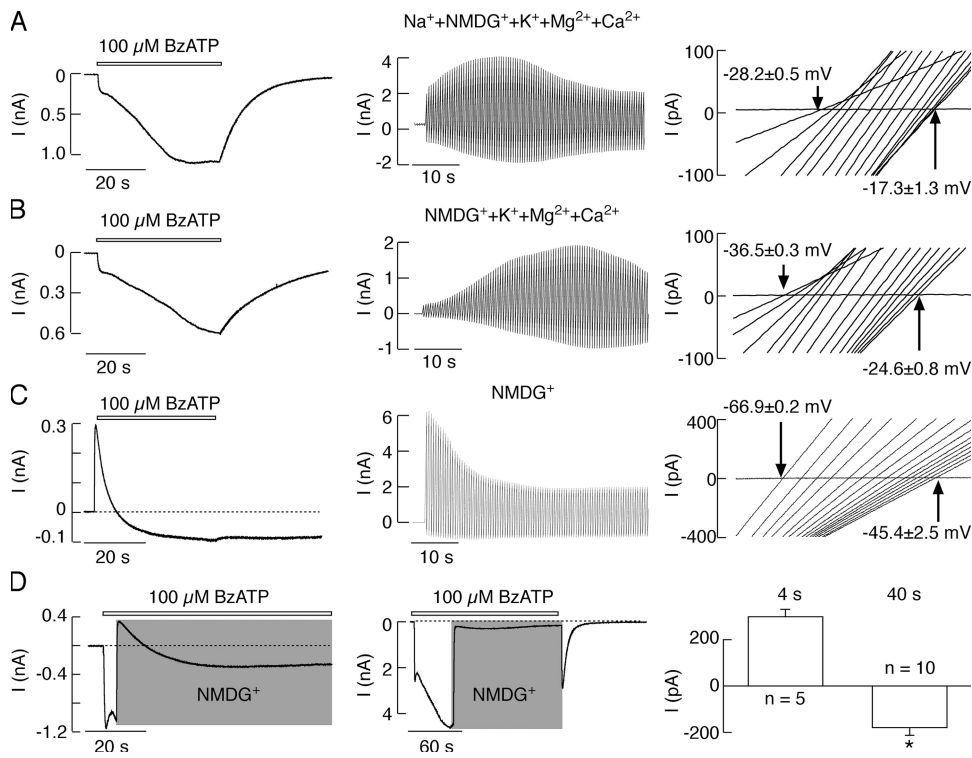
Figure 2. Permeability of P2X$_7$R to NMDG$^+$ depends on duration of agonist application. (A) Pattern of 100 µM BzATP-induced current and reversal potential in cells bathed in 10% Na$^+$ and 90% NMDG$^+$-containing KR buffer during the initial agonist application. (A, left) Current recording during a 40-s agonist application at −60 mV holding potential. (Middle) Time course of agonist-induced currents in cells under the ramp protocol. (Right) Positive shift in reversal potential observed during the initial 40-s application of BzATP; 0.485-s voltage ramps were delivered twice per second. (B) Patterns of BzATP-induced currents (left and middle) and shift in the reversal potential (right) in cells bathed in KR buffer, in which Na$^+$ was completely substituted with NMDG$^+$. (C) Time course of BzATP-induced P2X$_7$R current in cells bathed in NMDG$^+$ buffer (left and middle) and the accompanied changes in the reversal potential (right). In this and all figures, only 15 out of 100 traces for the current voltage relationship with the equal time intervals are shown. Notice the lack of receptor deactivation in C compared with records shown in A (left) and B (left). (D) Increase in NMDG$^+$ permeability occurs in cells bathed in physiological solution for agonist application of >∼10 s. Application of agonist was initially performed in cells bathed in KR buffer for 4 (left) and 40 s (middle) and was continued in NMDG$^+$ medium (gray areas). Notice a difference in responses when replacement of KR buffer with NMDG$^+$ buffer was performed during the phase I (left) and II (middle) of current growth. Right panel illustrates the mean ± SEM values of the peak currents reached after replacement of KR buffer with NMDG$^+$ buffer in two time points. All experiments were performed in HEK293 cells.

containing 100 µM BzATP. All recordings were performed at holding potential of −60 mV. After 4-s exposures to agonist, replacement of KR with NMDG$^+$ buffer induced a shift from inward to outward current in <1 s (Fig. 2 D, left). Once the peak was reached, the current again turned inward, with the time course highly comparable to that observed in cells bathed in NMDG$^+$ medium only (Fig. 2 C, left) and with similar amplitude of current (outward = 270 ± 19 pA; inward = −168 ± 31; $n = 5$). This is in accordance with published data (Jiang et al., 2005).

After a 40-s exposure to agonist, replacement of KR buffer with NMDG$^+$ buffer was also accompanied with a rapid decrease in the amplitude of inward current, but without reversing direction of current to outward (Fig. 2 D, middle); the amplitude of the peak current was −188 ± 28 pA and of the steady-state current was −394 ± 67 pA ($n = 10$). Furthermore, the steady-state current did not reflect nonreceptor-mediated permeabilization of cells because the washout of agonist with KR buffer induced a transient rise in current, followed by complete deactivation of channels (Fig. 2 D, middle). Thus, there was a significant difference in the peak current responses after replacement of Na$^+$-containing KR buffer with NMDG$^+$-containing buffer in

two experimental conditions (Fig. 2 D, right), and practically no difference in steady-state currents. These results indicate that the channel pore is permeable to NMDG$^+$ during sustained but not during initial phase of current growth.

Biphasic Current and Pannexin-1 Channels

P2X$_7$Rs operate as bi-functional molecules, and integration of pannexin-1 channels was suggested to account for cellular permeability to fluorescent dyes (Pelegrin and Surprenant, 2006). In general, the sustained rise in current could also reflect gradual integration of pannexin-1 channels into P2X$_7$R signaling. To test this hypothesis, we performed several experiments. Our reverse transcriptase–PCR analysis revealed that mRNA transcripts for pannexin-1 channels are expressed in GT1 and HEK293 cells (not depicted). In GT1 cells expressing P2X$_7$Rs, we also observed the uptake of YO-PRO-1. However, it required >200 s to approach saturation (Fig. 3 A), in contrast to biphasic current that leveled off within 30–70 s of stimulation with 100 µM BzATP in the same cell type (Fig. 3 C). Furthermore, the YO-PRO-1 uptake was observed in response to 100 µM ATP application (Fig. 3 A), a concentration that was unable
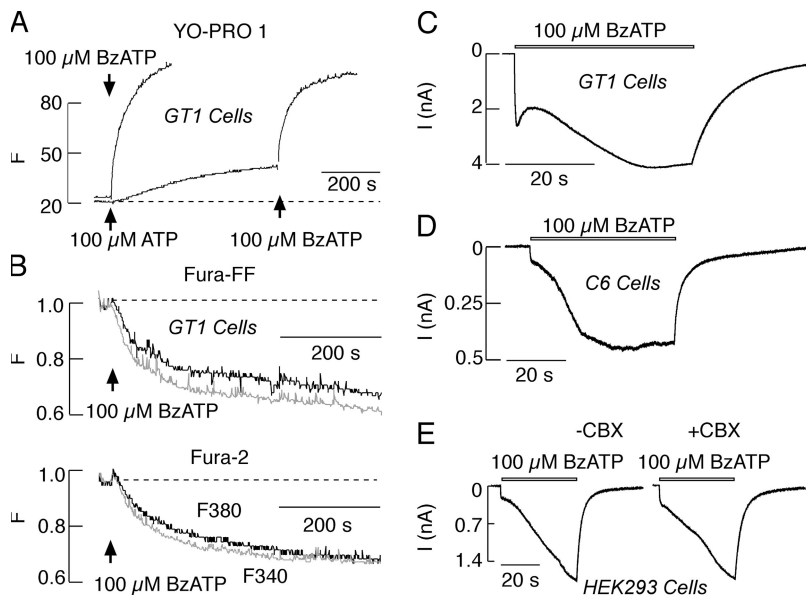
Figure 3. Agonist-induced biphasic current response is independent of pannexin-1 channels. (A) Agonist-induced diffusion of extracellular YO-PRO-1 into GT1 cells. Fluorescence intensities expressed in arbitrary units (λ_{ex} = 488 nm) are shown in response to application of BzATP only (left trace) and ATP followed by BzATP (right trace). (B) Normalized fluorescence intensities (gray, λ_{ex} = 380 nm; black, λ_{ex} = 340 nm) in GT1 cells loaded with Fura-FF (top) or Fura-2 (bottom) and stimulated with 100 µM BzATP. (C and D) BzATP-induced biphasic response in GT1 (C) and C6 single cells (D). (E) The lack of effects of CBX on pattern of current response in HEK293 cells; control (left) and 30 µM CBX-treated cells (right). In experiments shown in A, C, D, and E, cells were bathed in KR buffer. In experiments shown in B, cells were bathed in Ca^{2+}-deficient KR buffer.

to trigger the biphasic current. We also examined the leak of Ca^{2+} dyes Fura-FF and Fura-2 from cells. To eliminate changes in fluorescence induced by Ca^{2+} influx, cells were bathed in Na^+-containing/Ca^{2+}-deficient KR buffer. Under such ionic conditions, there was a progressive leak of Fura-FF and Fura-2 (Fig. 3 B) in response to 100 µM BzATP, as indicated by parallel changes in F_{380} and F_{340} signals, with leak rates comparable to the rate of YO-PRO-1 uptake.

The possible contribution of pannexin-1 channels in sustained current response was also evaluated in HEK293 cells expressing WT $P2X_7Rs$ by applying 30 µM carbenoxolone (CBX), an inhibitor of pannexin-1 channels, for 15 min. This treatment did not affect the pattern of biphasic response (Fig. 3 E); the ratio between the first and second phases of current, the latter measured at the end of the 40-s agonist application, was 1:2.38 for controls (1,036 ± 129 pA vs. 2,521 ± 208 pA; n = 7) and 1:2.38 for CBX-treated cells (874 ± 197 vs. 2,092 ± 215 pA; n = 7). To further test this hypothesis, we used C6 glioma cells as an expression system because these cells do not express pannexins endogenously (Lai et al., 2007). When transfected with WT $P2X_7Rs$, these cells responded with biphasic current during prolonged application of 100 µM BzATP (Fig. 3 D). These results indicate that endogenous expression of pannexins is not essential for sustained current growth. A delay in uptake and leak of fluorescent dyes could indicate a role of pannexin-1 channels in this process or that permeability of $P2X_7R$ channels for dyes reflects cell death and downstream effects.

A Role of the Y358-E375 C-terminal Sequence in Sustained Current Growth

Immediately after the second transmembrane domain, $P2X_7R$ contains a stretch of 18 amino acids, Y358–E375,

not found in other P2XRs. Deletion of this sequence (Δ18 mutant) was reported to affect conductivity for $NMDG^+$ (Jiang et al., 2005). In our hands, the mutant was unable to generate the biphasic current when cells were bathed in KR solution. The mutant initially responded to 100 µM BzATP with high amplitude of current that was reached rapidly, followed by a partial decline in the current amplitude during prolonged agonist application, and delayed deactivation after washout of agonist (Fig. 4 A, left trace). A similar pattern, but not amplitude of current, was observed in cells
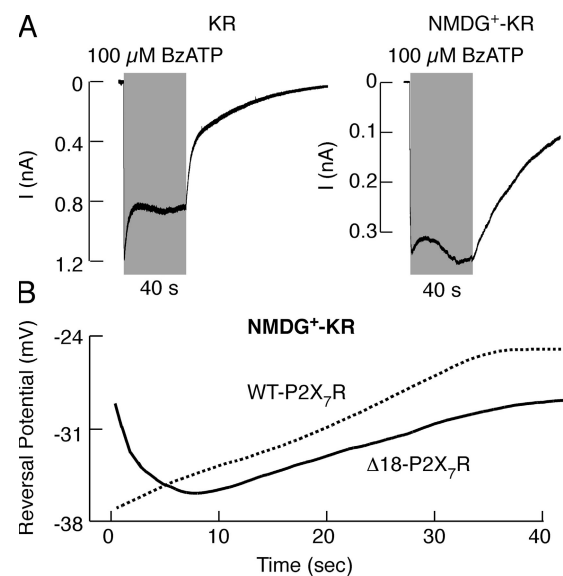
Figure 4. Effects of deletion of the $P2X_7R$-specific Y358-E375 C-terminal sequence (Δ18) on the pattern of current and permeability to $NMDG^+$. (A) Patterns of currents from cells bathed in normal (left) and $NMDG^+$-containing KR buffer (right). (B) Changes in the reversal potential during the 40-s application of 100 µM BzATP from cells perfused with $NMDG^+$-KR buffer.

perfused with NMDG[+]-KR buffer (Fig. 4 A, right trace). The reversal potential for this mutant at the beginning of agonist application was significantly shifted when compared with WT receptors, although recordings were performed in cells bathed in identical NMDG[+]-KR buffer (Fig. 4 B and Table I). Such a difference was also observed in cells perfused with NMDG[+] medium (-50.3 ± 0.9 mV for the $\Delta 18$ mutant vs. -66.9 ± 0.2 mV for the WT receptor; Table I), suggesting that the mutant was instantaneously permeable to organic cations. In further contrast to the WT receptor, this mutant initially showed a slow decrease in permeability to NMDG[+], which temporally coincided with a decline in the current amplitude, followed by a gradual recovery in NMDG[+] permeability during the 40-s agonist application (Fig. 4 B).

A Role of the Thr[15] Residue in Sustained Current Growth

All P2XRs have several putative protein kinase C phosphorylation sites, including the conserved 15TXK17 triplet of residues located in their N termini (P2X$_7$R numbering). We next tested whether phosphorylation of Thr[15] accounts for secondary current growth. Frequently, but not always, the introduction of Glu or Asp, or the introduction of positively charged residues, can mimic the effect of phosphorylation. In our experiments, cells bearing the T15E mutant responded to 100 µM BzATP, with a profile and amplitude of current comparable to that observed with the $\Delta 18$ mutant. Furthermore, the mutant was instantaneously permeable to NMDG[+] and NMEA[+], as indicated by reversal potential measured at the beginning of agonist application (Fig. 5 and Table I). In contrast to the $\Delta 18$ receptor, this mutant did not show additional changes in reversal potential during the 40-s agonist application. The permeability of cells expressing this receptor to YO-PRO-1 was not enhanced (not depicted), confirming that pannexin-1

channels do not account for increased permeability to NMDG[+]. Cells bearing the T15K mutant showed a similar pattern of current and permeability to NMDG[+] and NMEA[+] as the T15E mutant (Fig. 5 and Table I). Positive shifts in reversal potentials for the two mutants and the lack of biphasic responses suggest that the Thr[15] residue also contributes to the secondary rise in current amplitude, presumably in a protein kinase C–dependent manner.

However, additional experiments argued against a role for protein kinase C–dependent phosphorylation of Thr[15] for the generation of biphasic responses. Treatment of cells expressing the WT P2X$_7$R with phorbol ester PMA, a protein kinase C activator, did not affect the pattern of current during the initial agonist application (not depicted). Like the T15E and T15K mutants, the T15W mutant also responded to initial BzATP application with a monophasic current, and the receptor was instantaneously permeable to NMDG[+] and NMEA[+], even though tryptophan is not a charged residue (Fig. 5 and Table I). Finally, the K17A mutant responded to 100 µM BzATP with a biphasic current, and showed a gradual increase in the permeability to NMDG[+] and NMEA[+] in a manner almost identical to that observed in cells bearing the WT receptor (Fig. 5 and Table I), even though the putative phosphorylation site was removed.

We next substituted Thr[15] with valine and serine, as these amino acids are closest in structure to threonine. We also substituted this residue with smaller alanine. The T15V and T15S mutants responded to prolonged agonist application with biphasic currents. Permeability to NMDG[+] and NMEA[+] was reduced but not abolished in these mutants (Fig. 5 and Table I). The T15A mutant also responded to longer BzATP application by generating a biphasic current in cells bathed in KR buffer (Fig. 6 A), as well as in cells bathed in NMDG[+]-KR buffer

TABLE I
Permeability of the WT and Mutant P2X$_7$ Receptors to Organic Cations

Receptors	I (pA/pF) KR	RP (mV) NMDG[+]		RP (mV) NMDG[+]-KR		RP (mV) NMEA[+]-KR	
WT	122 ± 8	-66.9 ± 0.2	-45.4 ± 2.5^{b}	-36.5 ± 0.3	-24.6 ± 0.8^{b}	-20.0 ± 0.5	-4.6 ± 1.0^{b}
T15A	30 ± 3^{a}	-68.9 ± 0.4	-53.8 ± 1.2^{b}	-36.2 ± 0.8	-36.5 ± 0.5	-18.9 ± 0.7	-17.1 ± 1.1
T15E	94 ± 10	-54.9 ± 1.2^{a}	-53.7 ± 1.5	-22.4 ± 0.7^{a}	-21.8 ± 0.9	-14.8 ± 0.7^{a}	-12.0 ± 0.5
T15K	187 ± 45	-35.5 ± 0.9^{a}	-36.7 ± 0.6	-19.7 ± 0.6^{a}	-17.1 ± 0.6	-14.9 ± 0.5^{a}	-11.0 ± 0.6^{b}
T15W	142 ± 11	-52.6 ± 0.9^{a}	-47.4 ± 1.3	-23.0 ± 0.3^{a}	-22.4 ± 0.5	-16.4 ± 0.8^{a}	-14.4 ± 0.7
T15V	33 ± 4^{a}	-65.3 ± 0.6	-48.5 ± 1.9^{b}	-36.1 ± 0.3	-32.1 ± 0.6^{b}	-20.6 ± 0.4	-17.5 ± 0.5^{b}
T15S	47 ± 8^{a}	-65.8 ± 0.3	-53.4 ± 0.8^{b}	-36.6 ± 0.2	-31.7 ± 1.1^{b}	-20.9 ± 0.4	-12.9 ± 1.7^{b}
K17A	250 ± 25^{a}	-65.5 ± 0.4	-45.2 ± 3.6^{b}	-35.3 ± 0.2^{a}	-23.9 ± 1^{b}	-18.2 ± 0.6	-7.4 ± 0.4^{b}
$\Delta 18$	180 ± 21	-50.3 ± 0.9^{a}	-47.9 ± 1.2	-28.1 ± 0.6^{a}	-28.1 ± 1.1	-17.2 ± 0.4	-15.6 ± 1.1

Peak amplitude of current (I) reached during a 4-s agonist application and reversal potential (RP) for WT and mutant receptors bathed in KR, NMDG[+], NMDG[+]-KR, or NMEA[+]-KR solutions at the beginning (0.75 s; left columns) and end (right columns) of a 40-s application of 100 µM BzATP. Data shown are mean ± SEM values from at least six replicates per mutant.
[a]Significant differences between WT and mutant receptors during a 40-s agonist application; P < 0.01.
[b]Significant shifts in the reversal potential during a 40-s agonist application; P < 0.01.
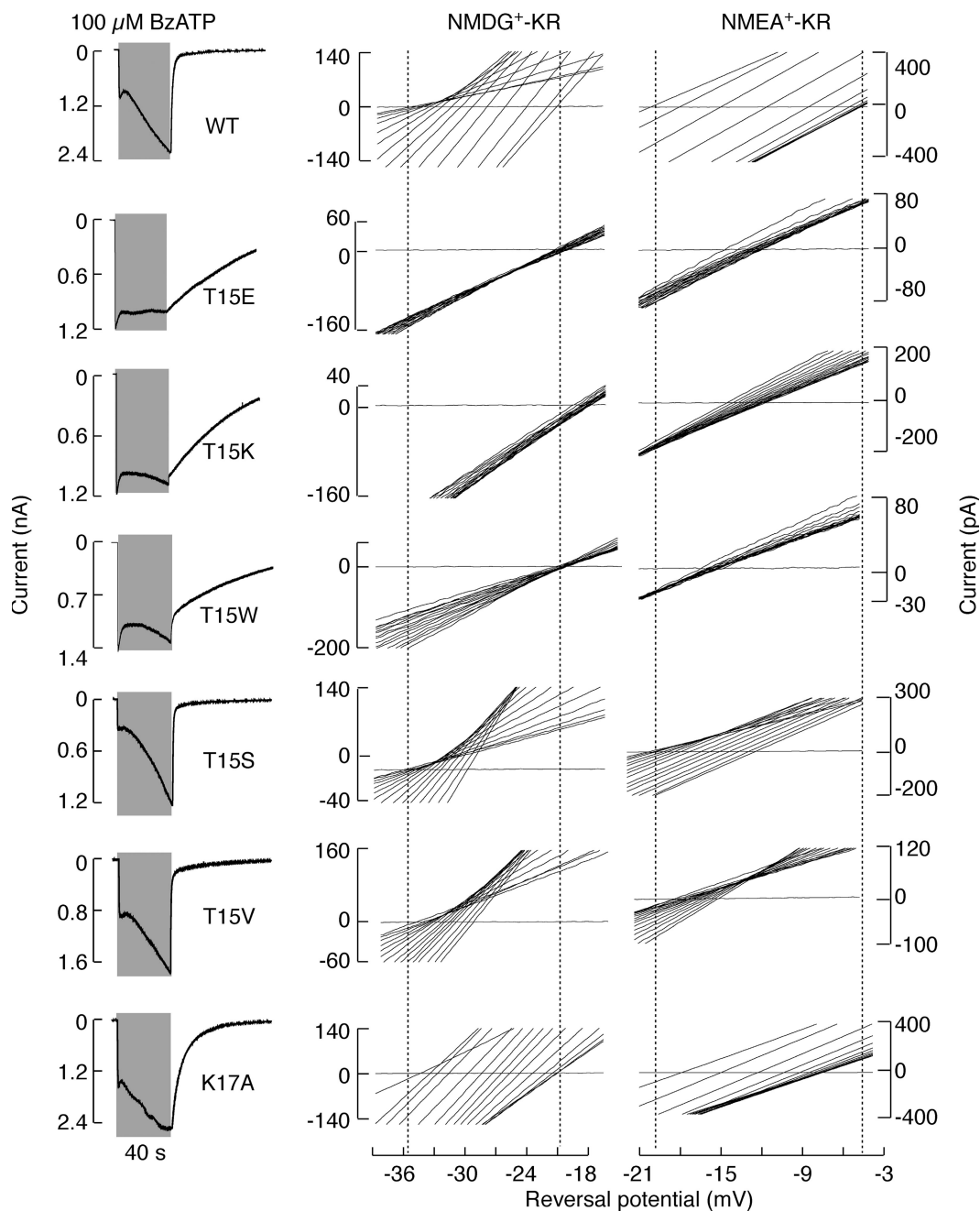
Figure 5. Characterization of N-terminal P2X₇R mutants. (Left) Representative traces of currents generated by a 40-s application of 100 μM BzATP by WT and mutant receptors expressed in HEK293 cells. Notice that BzATP induced monophasic currents in cells expressing T15E, T15K, and T15W mutants and biphasic current in all other mutants. Receptor deactivation was delayed in cells expressing T15E, T15K, T15W, and K17A mutants. Cells were bathed in KR buffer. (Middle and right) Comparison of the permeability of channels to NMDG⁺ (middle) and NMEA⁺ (right). Change in time courses are shown from left to right, and vertical dotted lines indicate the reversal potential for WT receptors at the beginning and at the end of a 40-s application of 100 μM BzATP. Cells were bathed in NMDG⁺- or NMEA⁺-containing KR buffer. Mean ± SEM values are shown in Table I.

(Fig. 6 B). As in control cells (Fig. 2 C, left), a rapid and transient outward current was observed in cells bathed in NMDG⁺ medium, followed by a shift from outward to inward current (Fig. 6 C). The initial reversal potential for this mutant bathed in NMDG⁺-KR and NMEA⁺-KR buffers was comparable to that observed in cells ex-

pressing WT receptors. In contrast to controls, prolonged application of agonist was not associated with a rightward shift in reversal potential (Fig. 6, D and E), indicating that the T15A mutant was not permeable to larger organic cations. In cells bathed in NMDG⁺ buffer, there was a positive shift in reversal potential by
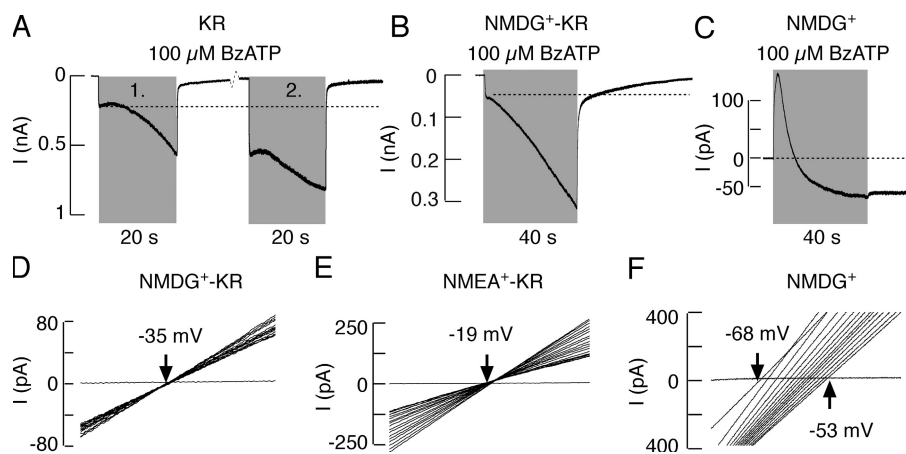
Figure 6. Characterization of the T15A-P2X$_7$R mutant expressed in HEK293 cells. (A) Patterns of current in response to repetitive application of 100 μM BzATP, followed by a washout period of 5 min. (B and C) 100 μM BzATP-induced biphasic response from cells bathed in NMDG$^+$-KR buffer (B) and NMDG$^+$ buffer (C). (D and E) Lack of channel permeability to NMDG$^+$ (D) and NMEA$^+$ (E) when cells were bathed in KR buffer in which all Na$^+$ was substituted with organic cations. (F) A shift in the reversal potential observed during a 40-s application of 100 μM BzATP from cells bathed in NMDG$^+$ medium.

+15.1 mV (Fig. 6 F) compared with the +22.5 mV shift observed in cells expressing the WT receptor.

DISCUSSION

Here, we have shown that the pattern of current response by rat P2X$_7$R at higher agonist concentrations is determined by the duration and the number of applications. Repetitive brief applications (2 s or less) of BzATP generated inward currents of highly comparable peak amplitudes. However, during the 4-s repeated agonist application, we consistently observed growth of current. Furthermore, in the continued presence of agonist, initial currents were always followed by slowly increasing currents, with time courses but not amplitudes determined by agonist concentration. Previous studies have also shown comparable amplitudes of P2X$_7$R current during repeated 2-s agonist applications (Hibell et al., 2000). Generation of biphasic currents during prolonged stimulation of cells expressing native and recombinant P2X$_7$Rs sometimes resulted in less clear separation of the two phases, probably reflecting the speed of application systems used (Chessell et al., 2001; Li et al., 2003; Ma et al., 2006). Biphasic current was also observed in P2X$_4$R when bathed in Ca^{2+}-deficient medium (Khakh et al., 1999), as well as in *Xenopus* oocytes expressing human P2X$_7$R (Klapperstuck et al., 2001). The occurrence of biphasic current response only at high agonist concentrations in our experiments is in accordance with a hypothesis of two distinct ATP activation sites at P2X$_7$R (Klapperstuck et al., 2001).

In general, the biphasic response could result from dilation of the integral ion channel pore that opens within milliseconds and/or from integration of pannexin-1 channels or another permeation pathway that opens more slowly. Our results are also consistent with the expression of native pannexin-1 channels in both HEK293 and GT1 cells. Furthermore, our data do not detract from previous work on the role of these channels in fluorescent dye uptake and their possible contribution to uptake/leak of fluorescent dyes during

activation of P2X$_7$Rs (Pelegrin and Surprenant, 2006). However, several lines of evidence presented here argue against the contribution of these channels or another permeation pathway to sustained current growth. First, the rates of leak of Fura-2 and Fura-FF were comparable to the rate of YO-PRO-1 uptake and slower than the time needed to reach the steady current during prolonged exposure to agonist. Second, the uptake of YO-PRO-1 occurs in cells stimulated with ATP in a concentration that was unable to generate the biphasic current. Third, C6 glioma cells do not express pannexin1–3 channels endogenously (Lai et al., 2007), but respond with generation of biphasic current during sustained agonist application. Fourth, the pattern of biphasic response was not altered in cells bathed in medium containing CBX, a pannexin-1 channel blocker. Consistently with our conclusions with P2X$_7$R, it has been shown recently that both sustained rise in P2X$_2$R current and permeability of channels to NMDG$^+$ are independent of pannexin-1 channels (Chaumont and Khakh, 2008).

In our experiments, the rates of sustained rise in current from cells bathed in KR buffer were highly comparable to the rates observed in cells perfused with Na$^+$/NMDG$^+$-KR and NMDG$^+$-KR media. Additionally, we observed that the rates of positive shifts in reversal potentials were comparable to the rates of delayed current growth in cells clamped at −60 mV. In previous reports, positive shifts in reversal potential during sustained agonist application in cells bathed in the presence of larger organic cations were used as indicators of the P2X$_7$R pore dilation (Khakh et al., 1999; Virginio et al., 1999; North, 2002). More recently, however, Jiang et al. (2005) questioned the hypothesis that P2XR pore dilation occurs under physiological conditions. The authors observed that replacement of Na$^+$ with NMDG$^+$ in activated cells caused the current to reverse its direction from inward to outward. They also found that deletion of a cysteine-rich 18–amino acid segment in the intracellular juxtamembrane region of the P2X$_7$R results in a mutant that is not permeable to NMDG$^+$ (Jiang et al., 2005). Single channel measurements also revealed the
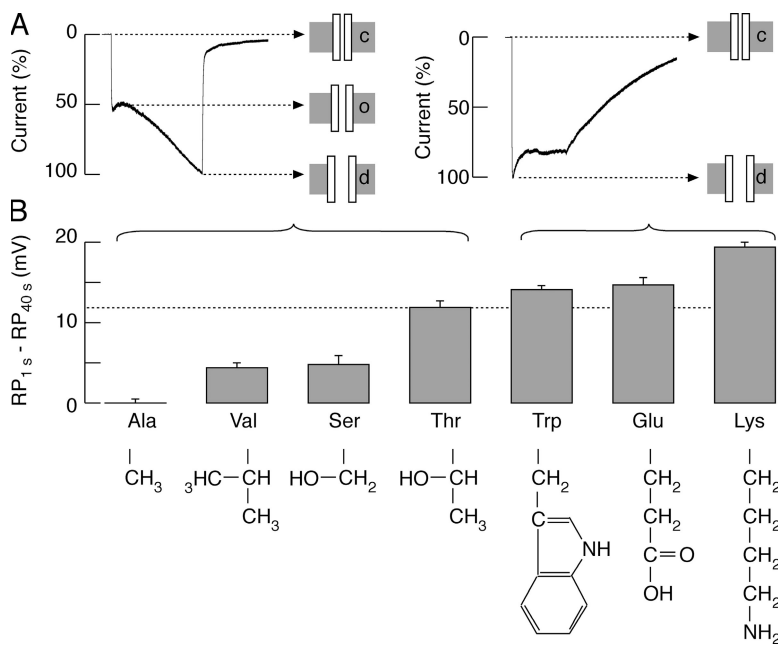
Figure 7. Effects of Thr[15] substitution on the pattern of current and permeability to NMDG$^+$ schematic models. (A) Two patterns of currents: biphasic (left) and high amplitude monophasic (right). The biphasic response reflects three steps in gating: closed (c), opened (o), and dilated (d), and is observed in cells expressing WT receptors and T15A, T15V, and T15S mutants. The high amplitude monophasic response reflects instantaneous transition from the closed to the dilated stage, and is observed in cells expressing T15W, T15E, and T15K mutants. (B) A shift in the reversal potential (RP) for WT and mutant receptors during sustained agonist application. Mean values for the reversal potential at the end of a 40-s recording for WT and six T15 mutant receptors were subtracted from the initial reversal potential value for the WT receptor (-36.5 mV; Table I, NMDG$^+$-KR column). The side chains of amino acid residues used in substitution studies are shown at the bottom.

lack of change in the channel kinetics during sustained activation of human P2X$_7$R expressed in *Xenopus* oocytes (Riedel et al., 2007a).

Consistent with Jiang's experiments, we also observed that substitution of KR buffer with NMDG$^+$ buffer after a short (4-s) exposure to 100 µM BzATP induced a shift from inward to outward current in <1 s. In contrast, when KR buffer was replaced with NMDG$^+$ buffer after a prolonged (40-s) application, the amplitude of inward current was dramatically reduced without shifting to outward current, with the mean value of current comparable to the steady-state current observed in cells continuously perfused with NMDG$^+$ medium for 40 s. In the absence of monovalent and divalent cations, the permeability of the channel pore for NMDG$^+$ resulted in the current amplitude of only 10% of that observed in controls. Such small amplitude of the whole cell current is consistent with the low permeability to Tris$^+$ observed in single channel recording with human P2X$_7$R (Riedel et al., 2007a). Furthermore, the Δ18-P2X$_7$R mutant in our hands showed an instantaneous positive shift in reversal potential when recording was performed in NMDG$^+$-containing medium both in the presence and absence of divalent cations, demonstrating that the initial opening of the channel pore of this mutant is larger than in controls. We also observed changes in permeability of this mutant during prolonged agonist application; an initial shrinking of the pore followed by sustained dilation. Collectively, these results suggest that the P2X$_7$R pore dilates during sustained agonist application, reaching the permeability for organic cations, and that the C-terminal influences this process.

In our experiments, three other P2X$_7$R mutants, T15E, T15K, and T15W, also showed instantaneous permeability to NMDG$^+$ and NMEA$^+$, whereas integration of pan-

nexin-1 channels requires time (Pelegrin and Surprenant, 2006). Changes in cation permeability for these mutant receptors reflected on the pattern of current response; all four generated high amplitude monophasic currents. The simplest explanation for changes in permeability to organic cations in cells expressing these mutants is that the channel pore immediately opens with the dilated mode, and that the diameter of the pore is sufficient to permit permeation of larger cations. In contrast to the Δ18 mutant, these three mutants stay locked in the initial dilated state. On the other hand, the biphasic response was preserved in cells expressing T15S, T15V, and T15A mutants. In the presence of divalent cations, the permeability of T15S and T15V receptors to NMDG$^+$ was significantly reduced, whereas the T15A mutant was not permeable to large organic cations. These results suggest the importance of N-terminal residues in pore dilation, but further experiments are required to clarify the residues of the relevance for this regulation and the structural details of conformation changes during pore dilation, and what extent pore dilation contributes to cell lysis. Consistent with our conclusion, it has been shown recently that P2X$_2$ receptors display permeability dynamics, which are correlated with conformational changes in the cytosolic domain remote from the selectivity filter itself (Chaumont and Khakh, 2008).

In summary, we suggest that channel pore opening of the WT receptor, as well as of the T15A, T15V, and T15S mutants, involves a two-step transition: (1) from closed to opened, and (2) from opened to dilated, leading to the generation of biphasic currents (Fig. 7 A). The steady-state size of the pore varies among these receptors, which is reflected by organic cation permeability (Fig. 7 B). In contrast, the enlargement of the channel

pore for T15E, T15K, and T15W mutants involves a single transition step, from closed to dilated, resulting in the generation of high amplitude monophasic currents (Fig. 7 A, right). In the absence of crystal structure data, it is difficult to predict how Thr[15] contributes to the control of gating. The T15XK17 triplet represents a putative protein kinase C phosphorylation site, but phosphorylation of the Thr[15] residue (if it occurs) does not account for delayed current growth. There is a parallel between changes in permeability of receptors to NMDG[+] and the steric size of the side chains of these residues (Fig. 7 B), suggesting that this phenomenon could underlie changes in the receptor behavior.

Edward N. Pugh Jr. served as editor.

REFERENCES

Chaumont, S., and B.S. Khakh. 2008. Patch-clamp coordinated spectroscopy shows P2X2 receptor permeability dynamics require cytosolic domain rearrangements but not Panx-1 channels. *Proc. Natl. Acad. Sci. USA.* 105:12063–12068.

Chessell, I.P., A.D. Michel, and P.P. Humphrey. 1997. Properties of the pore-forming P2X7 purinoceptor in mouse NTW8 microglial cells. *Br. J. Pharmacol.* 121:1429–1437.

Chessell, I.P., C.B.A. Grahames, A.D. Michel, and P.P.A. Humphrey. 2001. Dynamics of P2X7 receptor pore dilation: pharmacological and functional consequences. *Drug Dev. Res.* 53:60–65.

Dubyak, G.R. 2007. Go it alone no more–P2X7 joins the society of heteromeric ATP-gated receptor channels. *Mol. Pharmacol.* 72:1402–1405.

Egan, T.M., J.A. Cox, and M.M. Voigt. 2004. Molecular structure of P2X receptors. *Curr. Top. Med. Chem.* 4:821–829.

Ferrari, D., C. Pizzirani, E. Adinolfi, R.M. Lemoli, A. Curti, M. Idzko, E. Panther, and F. Di Virgilio. 2006. The P2X7 receptor: a key player in IL-1 processing and release. *J. Immunol.* 176:3877–3883.

Gudipaty, L., B.D. Humphreys, G. Buell, and G.R. Dubyak. 2001. Regulation of P2X(7) nucleotide receptor function in human monocytes by extracellular ions and receptor density. *Am. J. Physiol. Cell Physiol.* 280:C943–C953.

He, M.L., H. Zemkova, T.A. Koshimizu, M. Tomic, and S.S. Stojilkovic. 2003. Intracellular calcium measurements as a method in studies on activity of purinergic P2X receptor channels. *Am. J. Physiol. Cell Physiol.* 285:C467–C479.

Hibell, A.D., E.J. Kidd, I.P. Chessell, P.P. Humphrey, and A.D. Michel. 2000. Apparent species differences in the kinetic properties of P2X(7) receptors. *Br. J. Pharmacol.* 130:167–173.

Jiang, L.H., F. Rassendren, A. Mackenzie, Y.H. Zhang, A. Surprenant, and R.A. North. 2005. N-methyl-D-glucamine and propidium dyes utilize different permeation pathways at rat P2X(7) receptors. *Am. J. Physiol.* 289:C1295–C1302.

Khakh, B.S., X.R. Bao, C. Labarca, and H.A. Lester. 1999. Neuronal P2X transmitter-gated cation channels change their ion selectivity in seconds. *Nat. Neurosci.* 2:322–330.

Klapperstuck, M., C. Buttner, T. Bohm, G. Schmalzing, and F. Markwardt. 2000. Characteristics of P2X7 receptors from human B lymphocytes expressed in Xenopus oocytes. *Biochim. Biophys. Acta.* 1467:444–456.

Klapperstuck, M., C. Buttner, G. Schmalzing, and F. Markwardt. 2001. Functional evidence of distinct ATP activation sites at the human P2X(7) receptor. *J. Physiol.* 534:25–35.

Koshimizu, T.A., F. Van Goor, M. Tomic, A.O. Wong, A. Tanoue, G. Tsujimoto, and S.S. Stojilkovic. 2000. Characterization of calcium signaling by purinergic receptor-channels expressed in excitable cells. *Mol. Pharmacol.* 58:936–945.

Lai, C.P., J.F. Bechberger, R.J. Thompson, B.A. MacVicar, R. Bruzzone, and C.C. Naus. 2007. Tumor-suppressive effects of pannexin 1 in C6 glioma cells. *Cancer Res.* 67:1545–1554.

Li, Q., X. Luo, W. Zeng, and S. Muallem. 2003. Cell-specific behavior of P2X7 receptors in mouse parotid acinar and duct cells. *J. Biol. Chem.* 278:47554–47561.

Li, Q., X. Luo, and S. Muallem. 2005. Regulation of the P2X7 receptor permeability to large molecules by extracellular Cl- and Na+. *J. Biol. Chem.* 280:26922–26927.

Ma, W., A. Korngreen, S. Weil, E.B. Cohen, A. Priel, L. Kuzin, and S.D. Silberberg. 2006. Pore properties and pharmacological features of the P2X receptor channel in airway ciliated cells. *J. Physiol.* 571:503–517.

Michel, A.D., I.P. Chessell, and P.P. Humphrey. 1999. Ionic effects on human recombinant P2X7 receptor function. *Naunyn Schmiedebergs Arch. Pharmacol.* 359:102–109.

Nicke, A., H.G. Baumert, J. Rettinger, A. Eichele, G. Lambrecht, E. Mutschler, and G. Schmalzing. 1998. P2X1 and P2X3 receptors form stable trimers: a novel structural motif of ligand-gated ion channels. *EMBO J.* 17:3016–3028.

Nicke, A., D. Kerschensteiner, and F. Soto. 2005. Biochemical and functional evidence for heteromeric assembly of P2X1 and P2X4 subunits. *J. Neurochem.* 92:925–933.

North, R.A. 2002. Molecular physiology of P2X receptors. *Physiol. Rev.* 82:1013–1067.

Pelegrin, P., and A. Surprenant. 2006. Pannexin-1 mediates large pore formation and interleukin-1beta release by the ATP-gated P2X7 receptor. *EMBO J.* 25:5071–5082.

Petrou, S., M. Ugur, R.M. Drummond, J.J. Singer, and J.V. Walsh Jr. 1997. P2X7 purinoceptor expression in Xenopus oocytes is not sufficient to produce a pore-forming P2Z-like phenotype. *FEBS Lett.* 411:339–345.

Riedel, T., I. Lozinsky, G. Schmalzing, and F. Markwardt. 2007a. Kinetics of P2X7 receptor-operated single channels currents. *Biophys. J.* 92:2377–2391.

Riedel, T., G. Schmalzing, and F. Markwardt. 2007b. Influence of extracellular monovalent cations on pore and gating properties of P2X7 receptor-operated single-channel currents. *Biophys. J.* 93:846–858.

Smart, M.L., B. Gu, R.G. Panchal, J. Wiley, B. Cromer, D.A. Williams, and S. Petrou. 2003. P2X7 receptor cell surface expression and cytolytic pore formation are regulated by a distal C-terminal region. *J. Biol. Chem.* 278:8853–8860.

Surprenant, A., F. Rassendren, E. Kawashima, R.A. North, and G. Buell. 1996. The cytolytic P2Z receptor for extracellular ATP identified as a P2X receptor (P2X7). *Science.* 272:735–738.

Virginio, C., D. Church, R.A. North, and A. Surprenant. 1997. Effects of divalent cations, protons and calmidazolium at the rat P2X7 receptor. *Neuropharmacology.* 36:1285–1294.

Virginio, C., A. MacKenzie, F.A. Rassendren, R.A. North, and A. Surprenant. 1999. Pore dilation of neuronal P2X receptor channels. *Nat. Neurosci.* 2:315–321.

Yan, Z., Z. Liang, M. Tomic, T. Obsil, and S.S. Stojilkovic. 2005. Molecular determinants of the agonist binding domain of a P2X receptor channel. *Mol. Pharmacol.* 67:1078–1088.

Yan, Z., Z. Liang, T. Obsil, and S.S. Stojilkovic. 2006. Participation of the Lys313-Ile333 sequence of the purinergic P2X4 receptor in agonist binding and transduction of signals to the channel gate. *J. Biol. Chem.* 281:32649–32659.